Spatial, temporal and spectral structure of the turbulence-flow interaction at the L-H transition

T Estrada[1], E. Ascasíbar[1], E. Blanco[1], A. Cappa[1], P. H. Diamond[2], T. Happel[3], C. Hidalgo[1], M. Liniers[1], B. Ph. van Milligen[1], I. Pastor[1], D. Tafalla[1] and the TJ−II Team[1]

[1] Laboratorio Nacional de Fusión. Euratom-CIEMAT Association, 28040 Madrid, Spain
[2] University of California, San Diego, La Jolla, California 92093-0424, U.S.A.
[3] Max-Planck-Institut für Plasmaphysik, Euratom-IPP Association, 85748 Garching, Germany

E-mail: teresa.estrada@ciemat.es

Abstract. The physical mechanisms behind the L-H transition have been experimentally studied in the TJ-II plasmas. The spatial, temporal and spectral structure of the interaction between turbulence and flows has been studied close to the L−H transition threshold conditions. The temporal dynamics of the turbulence−flow interaction displays a predator−prey relationship and both, radial outward and inward propagation velocities of the turbulence−flow front have been measured. Moreover, the turbulence scales involved in the energy transfer of the predator−prey process have been identified.

PACS numbers: 52.35.Ra, 52.30..q, 52.55.-s

1. Introduction

The High confinement mode (H−mode) regime has been extensively studied since its discovery in the ASDEX tokamak [1]; however, the physical mechanism triggering the H-mode has still not been clearly identified. Bifurcation theory models based on the coupling between turbulence, zonal flows driven by the Reynolds stress, and equilibrium $E \times B$ flow, describe the Low to High confinement mode transition (L−H transition) passing through an intermediate, oscillatory transient stage [2, 3]. Zonal flows trigger the transition by regulating the turbulence until the mean shear flow is high enough to suppress turbulence effectively, which in turn subsequently impedes the zonal flow generation. Due to the self-regulation between turbulence and flows, the transition is marked by an oscillatory behavior with a characteristic predator−prey relationship [4] between turbulence and zonal flows.

This intermediate oscillatory transient stage, often called I−phase, has been seen in the L−H transition experiments in several devices. A dynamic behaviour of plasma parameters occurring near the L−H transition threshold conditions was first observed in the H−1 stellarator [5] and later in the DIII−D tokamak [6, 7] where experimental evidence was found supporting the predator−prey relationship between turbulence and flows as the basis for the L−H transition. More recently, this intermediate stage has also been observed in other devices: NSTX [8], TJ−II [9], AUG [10] and

EAST [11]. In these experiments, as in the predator−prey theory model [3], only the temporal dynamics of the turbulence−flow interaction is studied. However, as it has been pointed out in Ref. [12], where the 0−dimensional predator−prey theory model is upgraded toward a 1−dimensional one, the spatial evolution should also be taken into account as a necessary step to go towards the L−H transition model. This fundamental issue has been recently addressed in TJ-II [13] and also in DIII-D [14]. Besides, in TJ−II dedicate experiments have been carried out during the last experimental campaign to investigate the spectral structure of the turbulence−flow interaction during the predator−prey process.

In this work, after summarizing the spatiotemporal evolution of the turbulence−flow oscillation−pattern in section 2.1, its spectral structure is discussed in section 2.2.

2. Experimental results

The experiments have been carried out in the TJ−II stellarator (magnetic field $B_T = 0.95$ T, plasma minor and major radius $\langle a \rangle \leq 0.22$ m and $R = 1.5$ m, respectively), in pure NBI−heated plasmas (line−averaged plasma density $\langle n_e \rangle = 2 - 4 \times 10^{19}$ m^{-3}, central electron temperature $T_e = 300 - 400$ eV). The NBI input heating power is kept constant along the discharge but the fraction of NBI absorbed power −estimated using the FAFNER2 code that takes into account shine through, CX and ion losses− increases from 55 to 70% as the plasma density rises. TJ−II has a low, negative magnetic shear and the possibility to modify the rotational transform $\iota/2\pi$ within a rather broad range from 0.9 to 2.2. In these experiments the magnetic configuration is kept constant, the rotational transform at the plasma edge being equal to 1.53. As expected, consequence of the high rotational transform, no GAM oscillations have been detected in TJ−II to date. Due to the temporal and spatial scales involved in the L−H transition physics, specific experimental techniques are required to experimentally investigate the turbulence and flows dynamics [15]. In TJ−II, a two−channel Doppler reflectometer is used that allows the measurement of the $E \times B$ flow and density fluctuations at two radial positions simultaneously with good spatial and temporal resolution [16]. Besides, the Doppler reflectometer offers the possibility to probe different turbulence scales by steering the probing beam [17].

2.1. Spatiotemporal evolution

As reported in [9, 13], close to the L−H transition threshold conditions pronounced oscillations in both, E_r and density fluctuation level are measured at the plasma edge, right inside the E_r−shear position but not outside. As an example, figure 1 shows the time evolution of line−averaged plasma density, the estimated NBI absorbed power, the plasma energy content and the H_α signal together with the spectrogram of the Doppler reflectometer signal measured at $\rho \approx 0.8$. At about $t \approx 170$ ms the H_α drops, the plasma energy content and density increase and the spectrogram of the Doppler reflectometer signal shows an increase in its frequency and the onset of the oscillations. The oscillations appear as changes in the intensity and frequency of the Doppler reflectometry spectra, and show a predator−prey relationship between turbulence and flows, with the flow −the predator− following the turbulence −the prey− with a phase delay of 90° in a limit−cycle way. The repetition frequency of the oscillation−pattern changes along the plasma discharge as the line density increases.

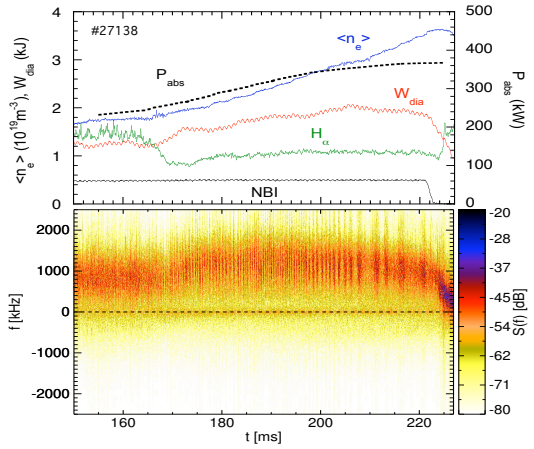

Figure 1. The time evolution of line-averaged plasma density, estimated NBI absorbed power, plasma energy content and H_α signal (top) and spectrogram of the Doppler reflectometer signal measured at $\rho \approx 0.8$ (bottom). At $t \approx 170$ ms the H_α drops, the frequency of the Doppler reflectometer signal increases and the oscillations start.

Besides, as the plasma density increases and the repetition frequency drops, the E_r oscillation amplitude decreases while that of the density fluctuation level increases. These observations can be explained based on the collisional damping of flows which eventually sets the turbulence level [18].

The radial profile of $E \times B$ flow changes from a rather flat profile in L−mode in the radial range from $\rho = 0.60$ to 0.85 to a sheared one during the oscillating I−phase with the $E \times B$ shear located at $\rho \approx 0.82$. In figure 2 the profile measured in L−mode and the extreme values of the flow oscillation measured at each radial position are displayed. The flow oscillation amplitude is about 1 km/s close to the $E \times B$ shear position and increases gradually as inner radial positions are probed. As a consequence, the E_r well of about 10 kV/m measured at the maximum of the oscillations shrinks in each limit−cycle and an inner shear layer is measured at $\rho \approx 0.75$ (see blue profile in figure 2). The TJ−II Doppler reflectometer allows measuring simultaneously at two radial positions which can be independently selected [19]. Therefore, it is possible to obtain information on the radial propagation characteristics of the cyclic spatio−temporal pattern. An example is shown in figure 3. It displays the time evolution of both, density fluctuation level (figure 3.a) and E_r (figure 3.b) measured simultaneously at $\rho = 0.8$ and $\rho = 0.75$. In addition, the time evolution of E_r−shear calculated from the data shown in figure 3.b is shown in figure 3.c. The relation between E_r−shear and density fluctuation level showing a limit−cycle behaviour is shown in figure 3.d. Pronounced changes in E_r−shear appear linked to the oscillations in $rms(\tilde{n}_e)$.

A delay between the two channels can be seen indicating a radial propagation from the inner to the outer channel. This outward propagation is found in all the oscillation−patterns measured at line−densities between $2 - 2.5 \times 10^{19}$ m^{-3}. At densities above 3×10^{19} m^{-3}, in some particular cases the propagation direction eventually reverses after a short time period without oscillations. The analysis of the delays yields propagation velocities within the range $\approx 50 - 200$ m/s with a

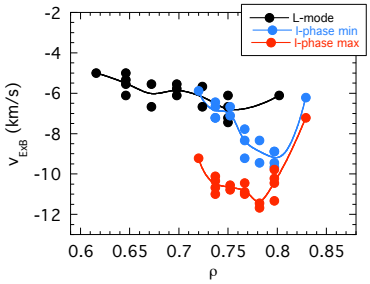

Figure 2. $E \times B$ flow profiles measured at L-mode (black) and during the intermediate oscillatory phase: flow maxima (red) and minima (blue).

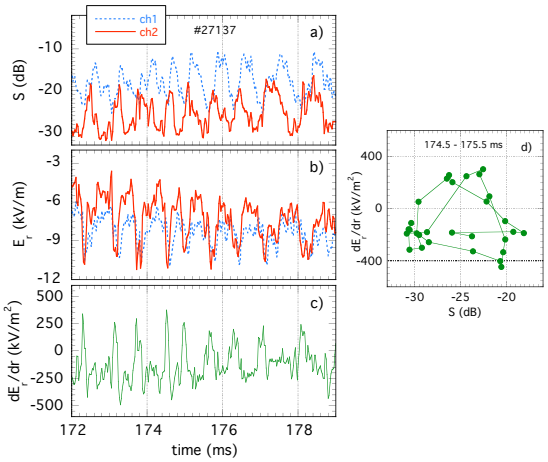

Figure 3. The time evolution of (a) density fluctuation level and (b) E_r, measured simultaneously at $\rho = 0.8$ (channel 1 in blue) and $\rho = 0.75$ (channel 2 in red). (c) the time evolution of E_r-shear and (d) relation between E_r-shear and density fluctuation level (only two cycles are displayed).

radial trend as shown in figure 4. In this figure the vertical bars represent the error in the estimation of the propagation velocity and the horizontal ones represent the radial separation between the two channels in each discharge. The radial propagation velocity decreases as the oscillation−pattern approaches the E_r-shear position (at $\rho \approx 0.82$). The inward propagation velocities are also included in figure 4. Similar values are obtained although no clear radial dependence can be inferred.

2.2. Spectral structure

The spectral structure of the turbulence−flow interaction has been measured during the intermediate oscillatory phase. To this end, the Doppler reflectometer ellipsoidal mirror tilt angle is scanned in a shot to shot basis to select different turbulence scales; at each tilt angle, measurements at different probing frequencies ensure a densely covered wavenumber−radial range. The wavenumber−radial range calculated using the three−dimensional ray tracing code TRUBA are shown in figure 5.left and the respective density profiles measured in L−mode at $n_e \approx 1.7 \times 10^{19} m^{-3}$ and during the I−phase at $n_e \approx 2 \times 10^{19} m^{-3}$ are sown in figure 5.right. The perpendicular wave-

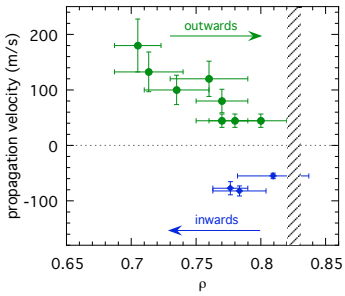

Figure 4. Radial propagation velocity vs. plasma radius. The outward propagation velocity decreases as the E_r-shear location (at $\rho \approx 0.82$) is approached. Inward propagation velocities are represented using *small* symbols (in blue). The striped area indicates the radial location of the E_r-shear.

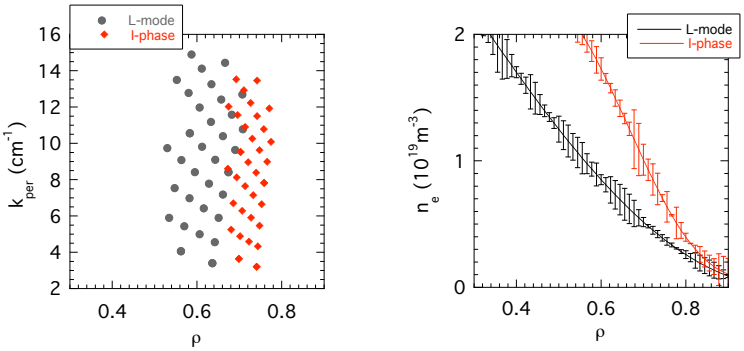

Figure 5. Left: Wavenumber − radial range covered by the Doppler reflectometer in L−mode (cicles) and during the intermediate oscillatory phase (diamonds). Right: Electron density profiles in L−mode and during the intermediate oscillatory phase.

number range covered in these experiments is: $k_\perp \approx 2 - 15$ cm^{-1}, the corresponding normalized wave-numbers being $k_\perp \rho_s \approx 0.4 - 3.0$.

Figure 6 shows the perpendicular wavenumber spectra of the density fluctuations measured during the L−mode, figure 6.left, and during the intermediate oscillatory phase, figure 6.right. During the I−phase, maxima and minima of the density fluctuation level are represented and labeled as S_{high} and S_{low}, respectively. In all cases, the density turbulence level decreases as the wavenumber increases and two wavenumber regions with different power laws and a well defined *knee*, can be identified. The spectral indexes and the wavenumber ranges are specified in the figure. In L−mode the spectral indexes are $\alpha = -2.7$ and -9.2 in the ranges $k_\perp < k_{knee} \approx 8.4$ cm^{-1} and $k_\perp > k_{knee} \approx 8.4$ cm^{-1}, respectively. Similarly, two different wavenumber ranges are found in the turbulence wavenumber spectra measured during the I−phase. A flatter wavenumber region is found in both cases at large turbulence scales, up to $k_{knee} \approx 5$ cm^{-1} in the low turbulence spectrum and up to $k_{knee} \approx 8$ cm^{-1} in the high one. At the *knee* the spectral fall−off starts with stronger spectral index in the high turbulence spectrum, $\alpha = -9.6$, as compared to that in the the low turbulence spectrum, $\alpha = -5.6$. The comparison between S_{high} and S_{low} shows a rather well defined wavenumber range where the oscillation in the turbulence level is maximum,

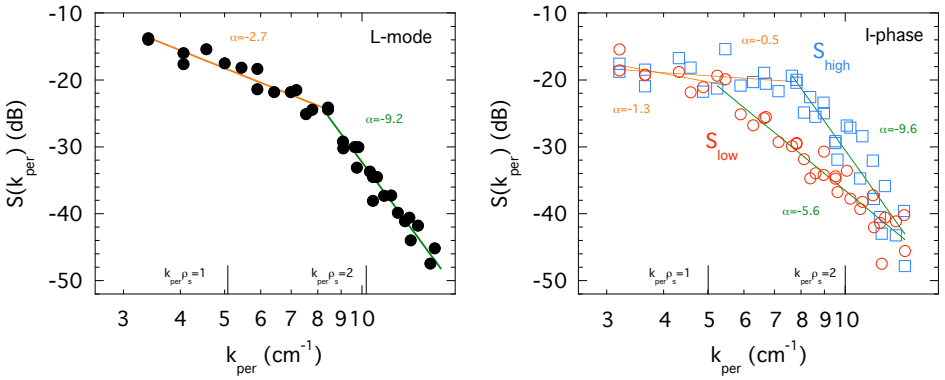

Figure 6. Density fluctuation wavenumber spectra measured during the L−mode at $n_e \approx 1.7 \times 10^{19} m^{-3}$ (left) and during the intermediate oscillatory phase at $n_e \approx 2 \times 10^{19} m^{-3}$ (right). The extreme values of the turbulence level measured during the I−phase are represented: maxima (*in blue*) and minima (*in red*). The spectral indexes are shown for each spectrum and the normalized wave-numbers $k_\perp \rho_s = 1$ and 2 are marked in the figures.

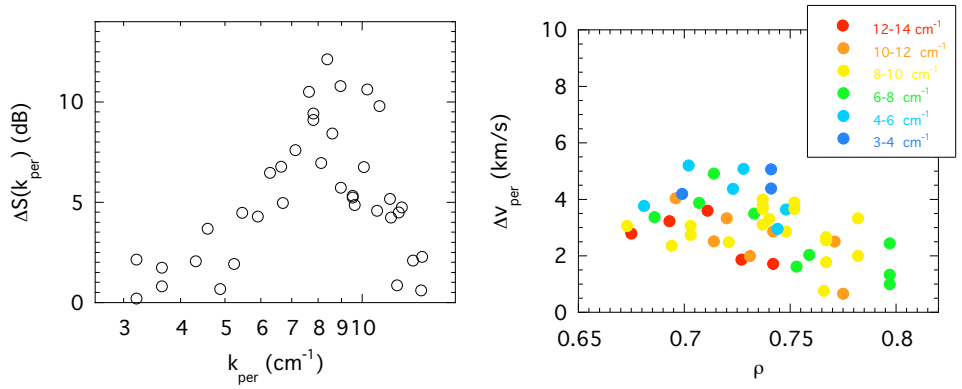

Figure 7. Left: Turbulence level oscillation amplitude, calculated as the difference between S_{high} and S_{low} (shown in figure 6.right), measured at different perpendicular wavenumbers during the I−phase. Right: $E \times B$ flow oscillation amplitude vs. plasma radius; perpendicular wavenumber intervals are color−coded

$k_\perp \approx 6-11$ cm^{-1}, the corresponding normalized wave-numbers being $k_\perp \rho_s \approx 1.2-2.2$. At shorter and longer scales, almost no oscillation in the turbulence level is detected. This is clearly seen in figure 7.left where the turbulence level oscillation amplitude, i.e. the difference between maxima and minima, is represented. The oscillation amplitude of the $E \times B$ flow is represented in figure 7.right. The flow oscillation amplitude is low, about $1-2$ km/s, close to the $E \times B$−shear position and increases at inner radial positions, in line with the $E \times B$ flow profiles shown in figure 2. No clear dependence of the flow oscillation amplitude with the turbulence scale is found.

3. Discussion and conclusions

The spatial, temporal and spectral structure of the turbulence−flow predator−prey interaction has been measured during the I−phase at the L−I−H transition in TJ−II plasmas.

Two distinct spatiotemporal patterns, namely outward and inward propagation, are measured. The outward radial propagation velocity gradually decreases as the oscillation−pattern reaches the E_r−shear position. In each oscillation cycle the E_r−well shrinks and an inner shear layer develops. A possible explanation for the spatio-temporal evolution of the oscillation−pattern could be linked to the radial spreading of the plasma turbulence from the plasma core to the edge barrier. As the turbulence propagates towards the barrier, the associated turbulence driven flow generates the inner shear layer which in turn regulates the turbulence level. The present observation could be also figured out in terms of turbulent bursts propagating toward the plasma edge. These turbulent bursts could be generated in the plasma interior due to instabilities linked, for instance, to the magnetic topology. To explain the present experimental observations, each turbulent burst should be accompanied on its way to the plasma edge by a sheared-flow layer. This observations resemble simulations results reported in [20], where the influence of shear flows on radially propagating turbulent transport events is investigated showing the damping of the transport events at the center of the barrier. Some similarities also arise from the comparison of our results and those found in a linear plasma device and reported in [21]. Those experimental results show how vortex-like structures propagating towards the plasma edge are slowed down and finally absorbed into the edge shear layer, transferring their momentum and energy to the shear flow which in turn is amplified. The inward propagation velocity of the oscillation−pattern is observed in some particular cases at the final stage of the discharge after a quiet period without oscillations. In those cases the oscillation−pattern arises at the outer shear layer position and propagates towards the plasma interior. Similar behavior has been recently reported in [14], where inward propagation velocities of about 200 m/s are measured inside the sepratrix position. The present experimental results indicate that the edge shear flow linked to the L−H transition can behave either as a slowing−down, damping mechanism of outward propagating turbulent−flow oscillating structures, or as a source of inward propagating turbulence-flow events.

The spectral structure of the turbulence−flow interaction has been measured during the I−phase allowing the identification of the relevant turbulence scales involved in the turbulence−flow predator−prey process. The measurements indicate that intermediate turbulence scales within the range $k_\perp \approx 6 - 11$ cm^{-1} dominate the process. This intermediate turbulence wavenumber range being the dominant player in the zonal flow generation by Reynolds stress has previously been identified both, experimentally [22, 23] and in simulations [24]. Besides, in previous experiments carried out at TJ−II, a scale−selective turbulence reduction was measured in H−mode in comparison with L−mode [17]. In H−mode, a turbulence reduction in the whole wavenumber range was measured, being more pronounced at intermediate scales. This observation together with the turbulence behavior found during the I−phase, and reported in section 2, are consistent with the bifurcation theory model of the L−I−H transition [3]. At the transition threshold conditions, a zonal flow driven by the turbulent Reynolds stress arises regulating the turbulence and given rise to the turbulence−flow predator−prey interaction. In this I−phase, the turbulence

is regulated mainly by the zonal−flow generation which effectively takes place at intermediate turbulence scales. No changes are measured at shorter and longer turbulence scales. As the plasma enters into the H−mode, additional mechanisms like turbulence decorrelation by sheared flows become active affecting a broader range of turbulence scales.

The reported experimental results support the predator−prey theory model of the L−I−H transition. The turbulence−flow front propagation and its interaction with the edge shear flow has been described and the turbulence scales involved in the energy transfer of the predator−prey process have been identified.

Acknowledgments

The authors acknowledge the entire TJ-II team for their support during the experiments. This work has been partially funded by the Spanish Ministry of Science and Innovation under contract number ENE2010-18409.

References

[1] F. Wagner *et al.*, Phys. Rev. Lett. **49**, 1408 (1982).
[2] P. H. Diamond, Y.-H. Liang, B. A. Carreras, and P. W. Terry, Phys. Rev. Lett. **72**, 2565 (1994).
[3] E.-J. Kim and P. H. Diamond, Phys. Plasmas **10**, 1698 (2003).
[4] V. Volterra, Nature **118**, 558 (1926).
[5] D. L. Rudakov, M. G. Shats, J. H. Harris, and B. D. Blackwell, Plasma Physics and Controlled Fusion **43**, 559 (2001).
[6] R. J. Colchin *et al.*, Phys. Rev. Lett. **88**, 255002 (2002).
[7] R. J. Colchin *et al.*, Nuclear Fusion **42**, 1134 (2002).
[8] S. J. Zweben *et al.*, Phys. Plasmas **17**, 102502 (2010).
[9] T. Estrada *et al.*, EPL (Europhysics Letters) **92**, 35001 (2010).
[10] G. D. Conway *et al.*, Phys. Rev. Lett. **106**, 065001 (2011).
[11] G. S. Xu *et al.*, Phys. Rev. Lett. **107**, 125001 (2011).
[12] K. Miki and P. H. Diamond, *Towards a 1D model of L-I-H evolution dynamics* (Asia Pacific Transport Working Group, Japan, 2011).
[13] T. Estrada, C. Hidalgo, T. Happel, and P. H. Diamond, Phys. Rev. Lett. **107**, 245004 (2011).
[14] L. Schmitz *et al.*, Phys. Rev. Lett. **108**, 155002 (2012).
[15] T. Estrada *et al.*, Plasma Phys. Control. Fusion **51**, 124015 (2009).
[16] T. Happel *et al.*, Rev. Sci. Instrum. **80**, 073502 (2009).
[17] T. Happel *et al.*, Phys. Plasmas **18**, 102302 (2011).
[18] Z. Lin *et al.*, Phys. Rev. Lett. **83**, 3645 (1999).
[19] L. Cupido, J. Sánchez, and T. Estrada, Rev. Sci. Instrum. **75**, 3865 (2004).
[20] P. Beyer, S. Benkadda, X. Garbet, and P. H. Diamond, Phys. Rev. Lett. **85**, 4892 (2000).
[21] M. Xu *et al.*, Phys. Rev. Lett. **107**, 055003 (2011).
[22] P. Manz, M. Ramisch, and U. Stroth, Phys. Rev. Lett. **103**, 165004 (2009).
[23] U. Stroth, P. Manz, and M. Ramisch, Plasma Physics and Controlled Fusion **53**, 024006 (2011).
[24] B. D. Scott, New Journal of Physics **7**, 92 (2005).